Nanosecond time resolution of electron-nuclear cross polarization within the optical nuclear polarization (ONP) process

1991 J. Phys.: Condens. Matter 3 6093

(http://iopscience.iop.org/0953-8984/3/32/015)

J. Phys.: Condens. Matter 3 (1991) 6093–6111. Printed in the UK

Nanosecond time resolution of electron–nuclear cross polarization within the optical nuclear polarization (ONP) process

G Buntkowsky†, D Stehlik†, H-M Vieth† and K M Salikhov‡

† FU Berlin, Institut für Experimentalphysik, Arnimallee 14, D-1000 Berlin 33, Federal Republic of Germany

‡ Zavoisky Physical-Technical Institute of the Academy of Sciences of the USSR, Sibirsky Trakt, 10/7, Kazan, 420029, USSR

Received 22 March 1991

Abstract. The spin dynamics of the generation of high nuclear spin polarization as a result of optical excitation (ONP) is studied with time resolution extending into the nanosecond range with the help of synchronized light and RF pulses. The well-characterized system—acridine doped into a crystalline fluorene matrix—has been used for the present dynamics study. With a short laser pulse, a selective sublevel population of the lowest acridine triplet state is generated. Resonant RF pulses of variable length initiate transfer of the electronic to nuclear spin polarization; the ONP-amplitude as a function of the RF pulse-length shows oscillating behaviour closely related to nutations of the electronic spins due to the resonant RF field. The ONP amplitude at the oscillation maximum is more than twice as high as the ONP level obtainable by CW RF-irradiation, which reflects an improved efficiency of the polarization transfer process. In contrast to the wide range of ONP experiments employing electron spins of stable paramagnetic systems the pulsed version of the ONP experiment permits direct time resolution of the electron nuclear cross-polarization process. In order to explain the results a two-step process is proposed and tested against the experimental data. In the primary step, the RF changes the spin order in the highly polarized electronic non-Zeeman reservoir in a similar way to hole-burning in a wide EPR line. This leads to a state which is far off equilibrium. In a second step, on a slower time-scale, the non-Zeeman reservoir re-equilibrates, mediated by electron nuclear spin-coupling causing the nuclear spins to be polarized. The process is compared with the thermal mixing concept as developed for dynamic nuclear polarization in solids with inhomogeneously broadened EPR lines.

1. Introduction

A standard technique to achieve high levels of spin polarization for systems with less favourable properties is to couple them to a more suitable spin reservoir and to transfer spin polarization from this to the spin reservoir of interest. Well-known examples are the dynamic nuclear polarization (DNP) [1–4] via the Overhauser effect [5], the solid effect [6], or thermal mixing [7–9], all of which utilize high electron spin order to polarize nuclear spins. Other cross-polarization techniques such as proton enhanced nuclear induction spectroscopy [10] transfer proton polarization to rare spin systems such as ^{13}C or ^{15}N. Optical nuclear polarization (ONP) [11, 12] can be seen as a related method in which the electronic spin order generated by optical pumping is used to generate strong

0953-8984/91/326093 + 19 $03.50

nuclear spin polarization. A unique advantage of the ONP scheme as compared to stable electron nuclear spin systems stems from the fact that the paramagnetic electron spin reservoir is generated by light and disappears with the characteristic decay rate of the optically excited state when the light is turned off. Light excitation also offers the possibility to devise time resolved versions of the ONP-experiment to study the spin dynamics of the electron nuclear cross-polarization process in a direct way, an option not available in the usual DNP experiments. With the ONP-experiment it thus becomes possible for the first time in our knowledge, to study the transfer of spin order between electronic and nuclear spin reservoirs with direct time resolution.

Time resolved cross-polarization studies are quite familiar for systems employing different nuclear spin reservoirs [13–19]. However, special features become important when an electron spin reservoir is involved.

(i) Due to the higher electronic magnetic moment the time scale of the dynamic processes is shifted to the nanosecond time scale.

(ii) The typically wide, inhomogeneously broadened EPR-lines allow only a non-uniform excitation contrary to the situation in most NMR experiments.

Consequently, different dynamical aspects are expected to be relevant in time resolved ONP-experiments. In recent reports [20, 21] we have demonstrated how a time-resolved version of ONP can be used to analyse the dynamics of electron–nuclear cross-polarization. Techniques with a time resolution of 10^{-9} s are required. In this time range characteristic oscillations are observed in the ONP amplitude as a function of the RF pulse duration. As a consequence the existing description of ONP has to be extended. While a semiclassical treatment—based on rate equations—has been sufficient so far [22–25], because the characteristic time-scale was 1 μs or longer, the analysis of fast dynamical processes must include coherence effects.

Already the qualitative analysis [20] indicates that the polarization transfer must occur as a two-step process. This is similar to some NMR-experiments where a polarization transfer between two spin reservoirs involves an intermediate spin order storage. In such NMR experiments [26] the common dipole–dipole reservoir of the different spin species was identified as this storage. In our case evidence can be given that the electronic non-Zeeman reservoir is the intermediate storage.

It is the aim of this paper to provide further experimental data with which a distinction of different mechanisms is possible and to develop a quantitative description of both the short-time behaviour of electron–nuclear polarization transfer and the cross-polarization process.

2. Method and experiment

2.1. Method

We begin with a brief description of the basic ONP scheme. For more details the reader is referred to Stehlik [12], Nack *et al* [27] and Vieth *et al* [28].

A salient feature is the use of a cyclic optical pumping process to generate electronic spin polarization repetitively and to transfer it to the abundant nuclear spin reservoir. The general ONP-scheme can be illustrated by a thermal reservoir concept as shown in

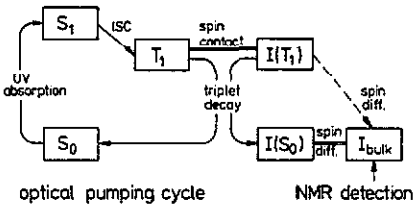

Figure 1. General scheme of energy transfer between reservoirs involved in the ONP process. The boxes within the optical pumping cycle represent the electronic energies of the electronic singlet ground state S_0, excited singlet state S_1 and the lowest excited triplet state T_1, respectively. The subreservoir T_1 includes also a spin energy of the unpaired electrons. The associated nuclear spin reservoirs are denoted with I.

figure 1. With respect to the increasingly slower time scales it can be separated in to the following different steps, which also provide the basis for the time resolved version outlined later.

(i) Excited triplet states T_1 of the guest molecules are optically pumped in a cyclic way. The rates of optical pumping from the S_0 ground state to the S_1 singlet state as well as of the ISC-process are usually very fast ($\leqslant 10^{-10}$ s) compared with all other time constants of the experiment (for acridine see [29]), therefore sudden generation of the triplet states can be achieved using a laser pulse. Due to the symmetry selection rules for the optical pumping and the ISC process, the electronic triplet spin states are populated highly selectively; electronic spin polarization (OEP) is generated.

(ii) During the lifetime of the triplet state RF may be irradiated near one of the triplet transitions thus driving the electronic spin system and changing its spin order. The time evolution will be governed by electron-magnetic interactions.

(iii) By electron–nuclear hyperfine coupling, polarization transfer can occur to the nuclei $I(T_1)$ coupled to the triplet state. Corresponding to the weaker HFS interaction strength a slower time regime is expected compared with that of the pure electron spin dynamics governed by stronger electron spin interactions.

(iv) The slowest time scale is associated with internuclear polarization transfer due to intramolecular and intermolecular dipole–dipole coupling, which distributes nuclear polarization. This polarization transfer may occur to some extent while the molecule is still in the excited triplet state, but mainly after the decay of the triplet. Note that triplet decay back to the singlet ground state as a purely electronic transition conserves nuclear polarization. Spin diffusion among the nuclei further distributes the nuclear polarization within the bulk nuclear spin reservoir of the host matrix. The optically active centre now is ready for another cycle.

After accumulating the effect of a sufficient number of optical excitation cycles the nuclear spin polarization is measured with a standard NMR pulse detection scheme.

Because nuclear spin lattice relaxation times are long in most molecular crystals, the polarization and the detection period can be fully separated in time, hence no receiver dead-time problems are encountered in observing the transient effects of the RF irradiation on the electronic spin system. Instead, limitations for the time resolution result only from the quality of the RF pulses and to some extent from the overall irradiation bandwidth during the polarization when the effects of light and RF irradiation are encoded into the spin reservoirs [27, 30].

2.2. *Experiment*

The experimental set-up resembles, in most parts, the RF-ONP instrumentation described earlier [28]. Hence, we will mainly describe the modifications.

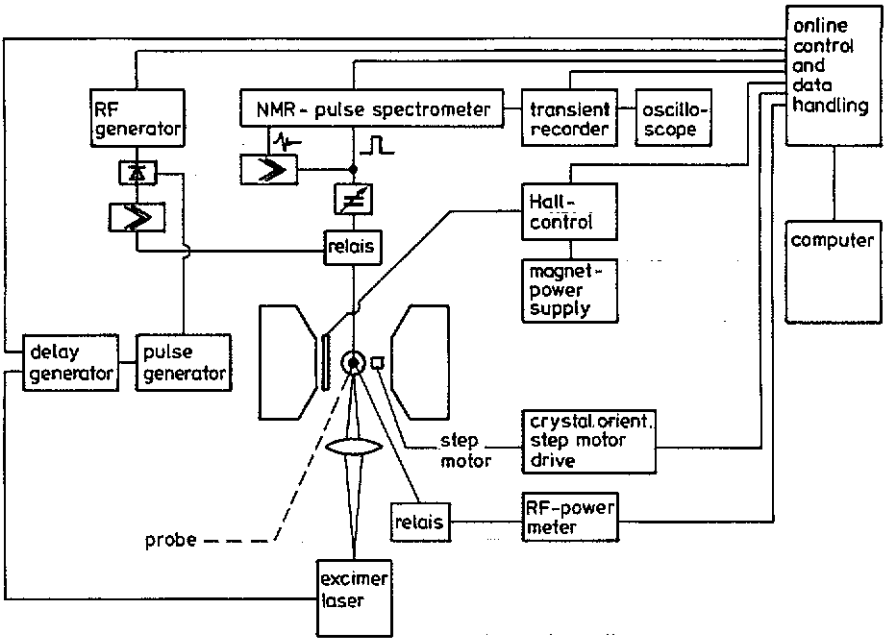

Figure 2. Block diagram of the ONP apparatus.

Figure 2 shows a block diagram of the apparatus. The detection unit consists of a fixed frequency solid-state pulse NMR-spectrometer with a home-built probe. The probe is customized to allow broadband irradiation of RF during the polarization phase and narrowband observation afterwards. The RF generated by a synthesizer is fed into a 200 W class A amplifier. Between synthesizer and amplifier is a high-speed electronic RF switch (1 ns switching speed) to generate the necessary pulses. The switch is controlled by a pulse generator with digital delay and with 1 ns resolution for the pulse width. The rise and fall time of the RF pulses is about 2 ns. With this equipment the total time resolution for the RF-irradiation part is 2 ns.

In order to analyse the oscillations it is important to determine the exact B_1-field strength of the RF irradiation. Therefore, we performed a careful calibration of the B_1 field for several frequencies. The procedure was as follows. A broadband pick-up coil was placed near the sample coil and the induced voltage monitored. We used the amplitude and width of a 180° pulse at the detection frequency of 30 MHz as a reference to calibrate the voltage U induced in the pickup coil against the B_1-field in the sample coil. The B_1-field at an arbitrary frequency ν is obtained from the linear relationship between the induction voltage and frequency,

$$B_1(\nu) = B_1(30\,\mathrm{MHz})[U(\nu)/U(30\,\mathrm{MHz})]\,30\,\mathrm{MHz}/\nu.$$

The light source for the optical pumping is an excimer laser (XeF line at 355 nm) or alternatively, an excimer pumped dye laser. The approximately Gaussian shape of the light pulses has a halfwidth of 15 ns. Since the triplet population rise time is much faster (50 ps) and the triplet decay time (250 μs) as well as the electronic spin lattice relaxation time (7 μs) much longer than the oscillation period, the time reference $t = 0$ for the

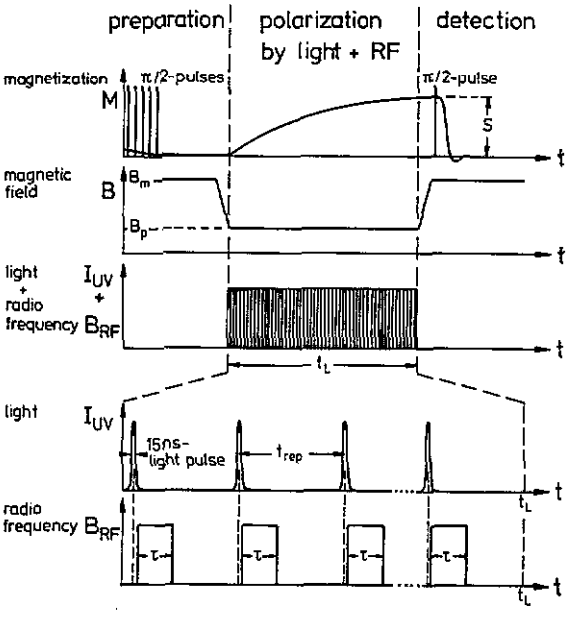

Figure 3. Time sequence of the pulsed RF-ONP experiment with the repetitive optical and RF pulses expanded at the bottom.

experiment is determined by the starting time of the RF irradiation. In this way, the shape and width of the light pulse do not limit the time resolution.

The complete time sequence of the experiment is shown in figure 3. The NMR pulses and the development of the nuclear magnetization, as well as the field cycling as shown in the upper parts of the figure, are the same as for the standard ONP experiments [12, 28]. At the beginning of the experiment the initial condition $P(0) = 0$ is set by destroying any existing nuclear magnetization by a string of resonant 90° pulses. After switching to the polarization field B_P the ONP is generated by irradiating repetitive sets of laser and RF pulses. The repetition time between two laser pulses is about 0.1 s to permit complete decay of the triplet states and to limit thermal damage of the sample by a low-duty cycle. The pulse sequence within each excitation cycle is shown in the lower two parts of figure 3. As already mentioned, in our case the zero-time reference point is defined to be the start of the RF irradiation. Therefore, consequences of jitter in the laser trigger and the effects of the laser pulse shape can be eliminated by a 40 ns delay between laser triggering and RF irradiation.

After averaging the polarization over a typical time period of about 30 s we switch back to the detection field B_m, and the ONP level is determined with the observed NMR signal amplitude following the detection pulse sequence. A switching time between the polarization field (about 45 mT) and the detection field (about 705 mT, which corresponds to a proton NMR frequency of 30 MHz) of about 10 s is still sufficiently short compared with typical nuclear spin lattice relaxation times in molecular crystals. Thus, any signal loss during the field cycling can be neglected. For improvement of the signal-to-noise ratio we use for detection a pulsed spin locking sequence [31]. The NMR-signal decay is digitized and stored in a transient recorder and later transferred to the computer for data processing.

Table 1. Parameters characterizing the triplet T_1 state of acridine-d_9 in fluorene.

Zero field splitting	Relaxation at $T = 300$ K
$D = 2209.8$ MHz [34]	$T_{1c} = 7\ \mu s$ [27] at $B_P = 42$ mT $\parallel c$-axis
$E = -261.6$ MHz [34]	$T_{2c} = 1.3\ \mu s$ [35]
Population selectivity	Lifetime and decay selectivity at $T = 300$ K†
$p_x = 0.906$ [36]	$\tau = 250\ \mu s$ [38, 39]
$p_y = 0.058$	$k_x = 0.333$ [27]
$p_z = 0.036$	$k_y = 0.333$
	$k_z = 0.333$

† Decay is preferentially due to the formation of photoproduct by *H*-transfer reaction with conservation of spin orientation.

By stepwise incrementation of the RF pulse duration between subsequent measurements the fast time evolution of the spin polarization is mapped out point by point with several hundreds of excitation cycles averaged for each RF pulse width. The oscillations can be analysed in the frequency domain after numerical Fourier transformation of the time signal. The width of the resulting line is determined by the damping of the oscillations.

In order to characterize the cross-polarization process several parameters are varied systematically: the B_1-field strength, the off-resonance term ΔB, the polarization field strength B_P and the light intensity. All data were taken at ambient temperature.

2.3. The molecular system

The experiments have been performed with the well-characterized system of fluorene doped with acridine. Details of the crystal structure are given in [32] and [33]. The ONP behaviour has been studied extensively [24, 25, 30]. While former investigations focus on very efficient ONP caused by a light induced radical pair, the data presented here refer to only the triplet state of the acridine guest molecules. The external magnetic field is aligned along the *c* axis of the fluorene crystal and thus along the long molecular in-plane axis of all molecules in the unit cell. Table 1 gives a summary of the relevant data characterizing the triplet state.

Favourable features of this system are the efficient population of the triplet state by the ISC and the highly selective triplet population [29, 36, 37]. The lifetime of the acridine triplet state in fluorene at 300 K is about 250 μs [38, 39] and permits fast repetition of the optical excitation cycle.

Maximum detection sensitivity could be achieved with fluorene which was deuterated except for its central methylene group. Comparison with protonated fluorene (Fl h_{10}) showed no differences in the ONP oscillations [20]. The partial deuteration allowed for proper crystal orientation along the magic angle during detection ($B_0 \parallel b$-axis) with efficient suppression of the intramethylene proton-dipole interaction. This results in long spin locking times and improved detection bandwidth.

The acridine guest molecules were fully deuterated (Ac–d_9). The concentration in the melt was 2000 ppm; crystals grown from the melt by the Bridgman technique contain a reduced concentration.

3. Model for the electron–nuclear cross-polarization process

3.1. Discrimination among various concepts

Coherence effects in cross polarization among different spin reservoirs are well known since the pioneering double resonance experiments in E L Hahn's laboratory [40]. In liquids, damped oscillatory transfer of the spin order shows a frequency that is determined by the magnitude of the J-coupling—the interaction responsible for the coupling between the reservoirs [19, 40]. The same process has been reported for solids with dipolar interaction as the coupling mechanism [17]. In our case, i.e. the transfer from electronic to nuclear spin order, the hyperfine coupling constitutes the relevant interaction. As concluded already in our earlier communication [20], the high value of the observed oscillation frequency as well as its independence of the hyperfine coupling prove this direct transfer process to be insignificant in the present experiment.

In addition, other types of oscillations have been observed in solid state NMR studies [13, 41, 42], which have frequencies varying with the RF field strength. Frequencies at γB_1 and $2\gamma B_1$ are observed corresponding to nutations of single and dipolar-coupled spins about the rotating RF field. The ONP transients clearly belong to this group of oscillations [20]. Here, an intermediate reservoir of spin order has to be involved, the time evolution of which is affected on the nanosecond time-scale by the RF irradiation; the short time scale indicates that it is of electronic origin.

In the theory of DNP the role of such intermediate reservoirs has been discussed in detail. So far only CW experiments could be carried out; therefore, descriptions based on the spin temperature concept for systems in thermal equilibrium are adequate and give excellent agreement between theory and experiment. This DNP mechanism is often referred to as thermal mixing [7, 9, 43–46]. Expanding these ideas, a refined model can be worked out, appropriate for our case of sequential preparation and mixing.

The starting point of the DNP concept is a cooling of the electronic spin–spin reservoir by an off-resonant CW RF field. More generally speaking, one considers the cooling of the electronic non-Zeeman reservoir [43]. This reservoir, which is well isolated from the electronic Zeeman system but tightly coupled (i.e. has an efficient thermal contact) to the reservoir of nuclear Zeeman energy [14, 47, 48] will therefore also cool the nuclear spins and thus lead to their polarization. As pointed out already by Kozhushner and Provotorov [49] and by Buishvili [50] in the mid-sixties, also in the absence of irradiation, this coupling can be effective.

In our case, as a result of the short and intense RF pulse the electronic non-Zeeman reservoir is left in a state far away from internal thermal equilibrium. The return to equilibrium which is called spectral diffusion requires, in general, an exchange of energy. This can involve nuclear spin energy in such a way that energy is balanced by simultaneous flips of electronic and nuclear spins.

Following this concept, we can calculate the energy content of the non-Zeeman reservoir at the end of the RF pulse as well as after re-establishment of thermal equilibrium. The energy difference is expected to be provided by the nuclear spin reservoir and to be proportional to the observed ONP.

3.2. Model calculations

In a simplified approach [51] the inhomogeneous EPR line is assumed to be composed of individual spin packets, which differ in frequency because of variations in the local

field—composed of zero-field splitting and hyperfine coupling to neighbouring nuclei. With the estimated concentration of the excited triplet states, the neglect of the intermolecular electronic dipole interaction as a contribution to the inhomogeneous linewidth seems justified; nevertheless, it plays an essential role in the process of thermal equilibration.

Using the notation of Abragam and Goldman [52] we write for the spin Hamiltonian of the inhomogeneously broadened electron spin system, including nuclear spins

$$\mathcal{H} = \omega_e S_z - \sum_k \Delta_k S_z^k \omega_n I_z + 2\omega_1 \cos \omega t S_x \tag{3.1}$$

where the first term describes the Zeeman interaction in the absence of inhomogeneities, the second term the inhomogeneous broadening, the third term the nuclear Zeeman coupling and the last term the interaction with the RF. The relative contribution of the spin packets of frequency Δ_k to the line is f_k with

$$\sum_k f_k = 1 \qquad \sum_k f_k \Delta_k = 0 \tag{3.2}$$

or by substitution of the sum by an integral

$$\int \Phi(\Delta)\, d\Delta = 1 \qquad \int \Delta\Phi(\Delta)\, d\Delta = 0 \tag{3.3}$$

$\omega_e = \bar{\omega}$ is the first moment of the distribution $\Phi(\Delta)$ describing the normalized EPR lineshape. As ω_e is more than one order of magnitude larger than Δ, it is justified to restrict consideration to the secular parts of zero-field splitting and hyperfine interaction as far as spectral position is concerned. Under neglection of the third triplet level, i.e. with the assumption of an effective spin $\frac{1}{2}$ system the electronic Zeeman energy has the value

$$\langle E_{EZ} \rangle = \tfrac{1}{2} N_e \omega_e \int \Phi(\Delta) P_z(\Delta)\, d\Delta \tag{3.4}$$

where N_e is the total number of molecules in one of these two triplet substates and $P_z(\Delta)$ the polarization of the spin packet at Δ

$$P_z(\Delta) = [n\uparrow(\Delta) - n\downarrow(\Delta)]/[n\uparrow(\Delta) + n\downarrow(\Delta)] \tag{3.5}$$

the electronic non-Zeeman energy is, in analogy,

$$\langle E_{ENZ} \rangle = -\tfrac{1}{2} N_e \int \Phi(\Delta) \Delta P_z(\Delta)\, d\Delta \tag{3.6}$$

and the nuclear Zeeman energy is

$$\langle E_{NZ} \rangle = -\tfrac{1}{2} N_n \omega_n P_n. \tag{3.7}$$

As the optical pumping leads to selective triplet sublevel population with respect to the electronic zero-field wavefunctions, we start with equal polarization $P(0)$ for all spin packets. Accordingly we find, directly after the light pulse

$$\langle E_{EZ} \rangle = \tfrac{1}{2} N_e \omega_e P(0) \tag{3.8}$$

$$\langle E_{ENZ} \rangle = 0 \tag{3.9}$$

and

$$\langle E_{NZ} \rangle = 0. \tag{3.10}$$

When the RF pulse is turned on, all spin packets start to precess around their local

effective field with the Rabi frequency $R(\Delta) = [(\omega - \bar{\omega} - \Delta)^2 + \omega_1^2]^{1/2}$. Thus, at the end of the pulse we are left with a new polarization distribution $P_z(\Delta)$ among the spin packets. A calculation analogous to the treatment of transient nutations [53] yields

$$P_z(\Delta, t) = P(0)[(1 - (2\omega_1^2/R^2(\Delta)) \sin^2(\tfrac{1}{2}R(\Delta)t)] \tag{3.11}$$

and $\langle E_{ENZ} \rangle$ after a pulse of length t becomes

$$\langle E_{ENZ} \rangle_t = P(0)N_e \int \Delta\Phi(\Delta)(\omega_1^2/R^2(\Delta)) \sin^2(\tfrac{1}{2}R(\Delta)t)\, d\Delta. \tag{3.12}$$

When, subsequently, the system approaches internal equilibrium, $\langle E_{ENZ} \rangle$ will again be negligibly small. Under the assumption that all the required energy exchange during this process proceeds exclusively with the nuclear Zeeman reservoir, we can write, for the resulting nuclear polarization,

$$P_n(t) = -\frac{2P(0)N_e}{N_n\omega_n} \int \Delta\,\Phi(\Delta)(\omega_1^2/R^2(\Delta)) \sin^2(\tfrac{1}{2}R(\Delta)t)d\Delta. \tag{3.13}$$

For sufficiently long pulses, when the oscillations are damped out, the time-independent level has the value

$$P_\infty(t) = -\frac{P(0)N_e}{N_n\omega_n} \int \Delta\,\Phi(\Delta)(\omega_1^2/R^2(\Delta))\, d\Delta. \tag{3.14}$$

$P_\infty(\omega)$ represents an expression for the ONP line in the CW RF-ONP experiment.

3.3. Spin-lattice relaxation and spectral diffusion rates

In our calculations spin-lattice relaxation effects have not been taken into account. This is a valid approximation for the duration of the RF pulse because the spin-lattice relaxation time $T_1 \approx 7\ \mu s$ and the spin–spin relaxation time $T_2 \approx 1.3\ \mu s$ (see table 1) are much longer than the pulse duration.

However, the competition between spectral diffusion and relaxation in the time range after the pulse poses a major concern and deserves more consideration. For good efficiency the polarization transfer to the nuclei has to be over before the electronic polarization P_z has substantially relaxed to the Boltzmann value. If the electrons relax via purely electronic spin flips with rate W_1 and all spectral diffusion processes are connected with nuclear spin flips with rate W_{SD}, then we have to reduce the nuclear polarization from (3.13) by the branching ratio $W_{SD}/(W_1 + W_{SD})$.

Two major processes for nuclear spin flips under the influence of paramagnetic centres have been discussed in the literature. The first is the simultaneous flip of one electronic and one nuclear spin. It involves a large change $\hbar(\omega_e - \omega_n) \approx \hbar\omega_e$ of energy, which has to be exchanged with the lattice. The rate W_{SI}^{jk} for the joint flip of nucleus k and electron j due to hyperfine coupling can be related to the electronic relaxation rate W_1 [54].

$$W_{SI}^{jk} = W_1(|B^{jk}|^2/\omega_n^2) \tag{3.15}$$

where the interaction parameter B^{jk} derives from the term $\hbar(B^{jk}S_z^jI_+^k + B^{*jk}S_z^jI_-^k)$ in the dipolar coupling between electron j and nucleus k.

The second process is a three-spin process, a flip-flop of two electron spins accompanied by one nuclear spin flip. Here, the corresponding energy quantum is $\hbar(\omega_{e_1} - \omega_{e_2} - \omega_n)$, which can be zero; in this case no energy exchange with the lattice

is necessary. In a perturbation treatment the rate W_{SD}^{jmk} for the three-spin process can be related to the electronic spin–spin relaxation [54]

$$W_{SD}^{jmk} = (W_{SS}^{jm}(|B^{jk}|^2/\omega_n^2))\Phi(\omega_n)/\Phi(0) \tag{3.16}$$

where W_{SS}^{jm} is the probability for a flip-flop transition of the dipolar coupled electron spins j and m.

As our experiments are done at relatively low fields, the ratio $|B^{jk}|^2/\omega_n^2$ can be large for nuclei close to the electronic spin, even to the extent that the perturbation treatment is no longer allowed. Nevertheless, it should provide the right order of magnitude. With $T_{2e} \sim 1.3\ \mu s$ a spectral diffusion time between 5 and 20 μs seems realistic. This is in line with our result: that the polarization transfer efficiency is independent of the light intensity; whereas insufficiently slow spectral diffusion would show up as a bottleneck of the cross-polarization process, i.e. as a non-linear dependence of ONP on light intensity.

In comparison, the energy exchange between the nuclear Zeeman reservoir and the rotating frame electron Zeeman reservoir, corresponding to the term $\omega_1 S_x$ in (3.1) is expected to proceed on a significantly slower time-scale, and thus can be neglected for RF pulses below 1 μs. Energy quanta near ω_1 are exchanged in this process, which therefore has a characteristic time constant of the order of $T_{1\rho}$. In addition, the energy is limited to the time with the RF switched on. After the pulse, this energy decays fast because of dephasing processes. Hence, only for very long RF pulses when all oscillations are over is such an effect observable.

Polarization $P_x(\Delta, t)$ parallel to the B_1 field builds up due to RF irradiation off-resonance. In analogy to (3.11) one obtains

$$P_x(\Delta, t) = P(0)[(2\omega_1\Delta/R^2(\Delta))\sin^2(\tfrac{1}{2}R(\Delta)t)] \tag{3.17}$$

and for the corresponding energy E_{ERZ}

$$\begin{aligned}\langle E_{ERZ}\rangle_t &= -P(0)N_e\omega_1 \int \Phi(\Delta)P_x(\Delta, t)\,d\Delta \\ &= -P(0)N_e \int \Delta\Phi(\Delta)(\omega_1^2/R^2(\Delta))\sin^2(\tfrac{1}{2}R(\Delta)t)\,d\Delta \\ &= -\langle E_{ENZ}\rangle_t. \end{aligned} \tag{3.18}$$

The ONP contribution resulting from a pulse of length τ is proportional to

$$-\int_0^\tau \langle E_{ENZ}\rangle_t\,dt. \tag{3.19}$$

As this term has an opposite sign with respect to the non-Zeeman term, the ONP signal for long pulses is expected to include a component decaying with a time constant of about $T_{1\rho}$.

3.4. Numerical procedure

For quantitative calculations, the shape $\Phi(\Delta)$ of the EPR line has to be modelled. From comparison with the CW-ONP measurements (see figure 4) a shape close to a Gaussian

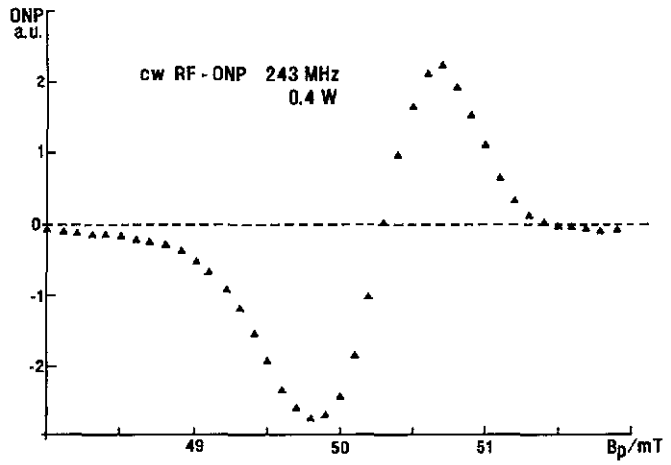

Figure 4. Reference RF-ONP spectrum with CW irradiation of light and RF at fixed frequency of 243 MHz.

seems appropriate, modified by some asymmetry, as characterized by an asymmetry parameter α ($\alpha = 0$: symmetric case)

$$\Phi(\Delta + \bar{\Delta}) = N \exp[-(1 + (\alpha/\pi)\arctan(\Delta + \bar{\Delta}))2(\Delta + \bar{\Delta})^2/\Delta_{pp}^2] \tag{3.20}$$

with the normalization constant N, such that $\int_{-\infty}^{\infty} \Phi(\Delta)\, d\Delta = 1$. To take relaxation effects into account (e.g. spin lattice relaxation, T_2 relaxation, and dephasing due to inhomogeneous B_1) we multiplied the oscillations with a Gaussian damping function. We determined the appropriate width from the experimentally observed decay of the transients for irradiation at low frequency offset.

4. Results

4.1. ONP data

It is obvious that the ONP level strongly depends on the electronic spin order in the triplet state, hence it is necessary to determine the electronic polarization for the chosen magnetic field values B_p around 50 mT with $B_p \| c$. Figure 4 shows the RF-ONP signal of the acridine $T_1|0\rangle \rightarrow |+\rangle$ transition at 243 MHz in a field sweep experiment under CW irradiation at low RF power (0.4 W) to avoid line broadening. A dispersion-like line shape is observed, which is characteristic for spectra owing to a non-resolved solid-state effect consisting of two lines with opposite signs from two forbidden ESR transitions [28, 55]. The transitions to the $|-\rangle$ level are far off-resonance and not excited by the RF. Hence, for the analytical description of the polarization transfer the use of an effective two-level system for the electron spin is justified. It may be mentioned that at the chosen polarization field any background ONP signal due to mixing of states, as found near level crossing regions (LAC-ONP) [12], can be ignored, i.e. proton polarization without RF irradiation is negligible. After integration of the observed RF-ONP line the line-shape of the inhomogeneous ESR absorption profile is obtained in good approximation. The profile determines also the population difference of the spin substates as a function of

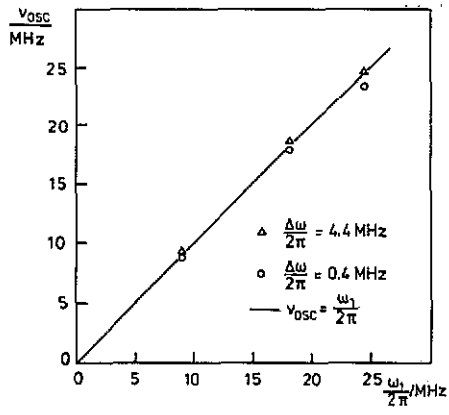

Figure 5. Frequency ν_{osc} of transient ONP oscillations with the polarization field $B_P \| c$ as a function of the RF field strength B_1 (in frequency units of $\omega_1/2\pi = \sqrt{2}\,\gamma_e B_1/2\pi$).

the field. It turns out to be close to a Gaussian line of 0.8 mT peak-to-peak width with a slight asymmetry.

As it is the primary concern of this paper to provide a detailed analysis of the first step of the polarization transfer, we measured the oscillatory ONP time evolution under a systematic variation of several RF irradiation parameters.

Previous measurements [20] had already given evidence that the direct coupling process via hyperfine interaction can be excluded; the comparison between systems with protonated and deuterated acridine guest molecules showed no significant differences in the oscillations. In order to distinguish the alternative cross-polarization mechanisms discussed in section 3 the role of the different spin energy reservoirs involved has to be clarified. One characteristic property to discriminate the coherent time evolution of the spin order between different reservoirs is the frequency of the observed oscillations under the influence of the B_1 field. Near resonance, one finds for the Zeeman order in the rotating frame the frequency $\omega_1 = \gamma B_1$ of Torrey nutations, while for the dipolar order frequency components around $2\omega_1$ are also expected [41, 42].

In all our measurements with irradiation near the centre of the EPR line we observed a strict proportionality between oscillation frequency ν_{osc} and RF amplitude B_1 as shown in figure 5. Within the accuracy of our RF field calibration ($\pm 7\%$) the factor of proportionality is $\gamma = \sqrt{2}\,\gamma_e$ where the $\sqrt{2}$ factor is due to the effective spin $\frac{1}{2}$ case, when we selectively drive only the transition between two out of the three triplet levels. As no frequency contributions are observable near the double frequency we can say that the electronic dipole spin reservoir does not play a significant or direct role in the dynamics of the primary cross-polarization step. This is not surprising when considering the low concentration of optically populated triplet states in the sample, which remains considerably below the already small doping concentration of 2000 ppm as will also be seen from measurements at different light intensities (see below).

In order to study the effects due to the vicinity of a triplet level crossing ($B_{LC} = 39.6$ T), where strong mixing of states occurs, we compared ONP oscillations at fields B_P between 41.0 mT and 47.7 mT, corresponding to resonance frequencies between 30 MHz and 180 MHz. No deviation of the oscillation frequency from $\omega_{osc} = \sqrt{2}\,\gamma B_1$ was observable, neither could a significant change of the ONP amplitude be seen. As a consequence we could apply a fixed radio frequency of 120 MHz for which the maximum RF power was available.

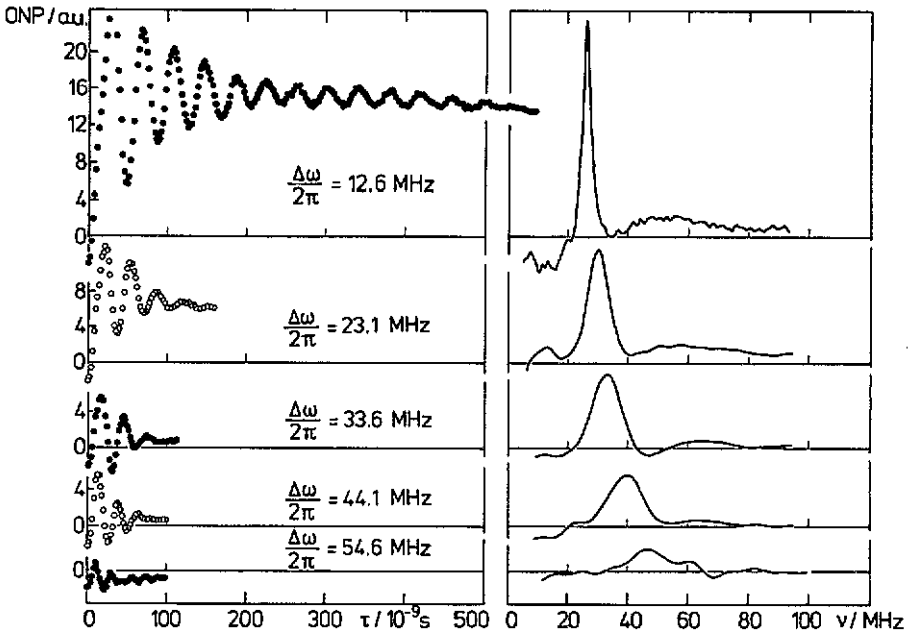

Figure 6. ONP oscillations observed at different off-resonance settings $\Delta\omega/2\pi$ with the RF field amplitude corresponding to $\omega_1 = 2\pi\,25$ MHz. Oscillatory time evolution (left) and Fourier analysis (right).

Frequency and amplitude of the oscillations depend on the off-resonance setting $\Delta\omega = \omega_{RF} - \bar{\omega}$. Figure 6 compares ONP oscillations for five different values of $\Delta\omega$ and constant ω_1 ($2\pi 25$ MHz), in the time domain (left part) and after Fourier transformation (right part: phase corrected absorption spectrum; the components near zero are suppressed; the spectral lines have different amplitude scaling). With increasing $\Delta\omega$ the oscillation frequency increases, the damping accelerates and the maximum ONP amplitude reaches its highest values for $\Delta\omega$ near the half-width of the inhomogeneous EPR line. Changing the sign of $\Delta\omega$ corresponds to a 180° phase shift of the oscillations, accordingly the ONP stays near zero for $\Delta\omega \approx 0$. A more subtle effect is the initial phase, which changes from a cosine behaviour for $\Delta\omega \approx 0$ to a sine phase at higher $\Delta\omega$ values.

In figure 7 the centre frequencies of the Fourier transform, ν_{osc}, are plotted as a function of $\Delta\omega$ and compared with the Rabi frequency $\omega_R = [\omega_1^2 + (\Delta\omega)^2]^{1/2}$, which is expected for the Torrey nutation of a spin ensemble in a homogeneous effective field. The oscillation frequency stays near ω_1 up to values of $\Delta\omega$ larger than the half-width of the inhomogeneous line ($\frac{1}{2}\Delta_{pp} = 11.1$ MHz). Only when going further off-resonance does the frequency start to increase, but stays in all cases (except for $\Delta\omega = 0$) well below the Rabi frequency. The width of the Fourier transform line, i.e. the damping of the oscillations, increases with larger values of $\Delta\omega$. No effects on the width due to insufficient B_1-homogeneity have been found.

For pulse durations longer than 1 μs an exponential decay is observed which results from the polarization component P_x parallel to the RF field as discussed in section 3.3 (see figure 8). The decay time of about 7 μs demonstrates that the transfer from the electronic rotating-frame Zeeman reservoir to the nuclear spins is, at least for $B_{local} < B_1$, limited by T_{1e}.

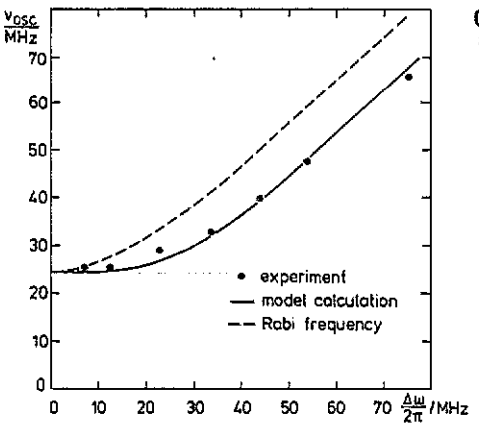

Figure 7. Comparison of observed (·) and calculated oscillation frequencies (full curve). The experimental points are the peak positions of the Fourier transform spectra (figure 6). The broken curve represents the Rabi frequencies for a homogeneous line.

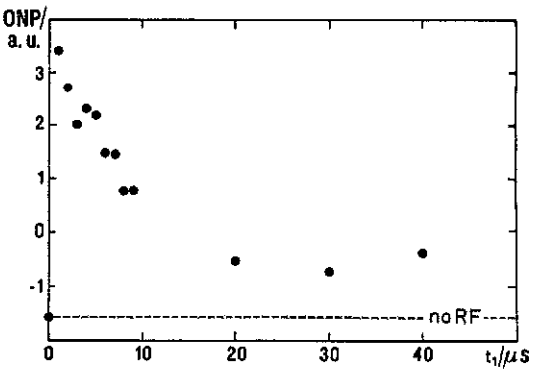

Figure 8. ONP time evolution for long RF pulses ($\tau > 1\ \mu s$). RF field strength $\omega_1 = 2\pi$ 16 MHz; transition frequency $\nu = 120$ MHz.

In figure 9 the ONP amplitude is given as a function of the polarization field B_p for long pulse duration when the oscillations are damped out. Overall, the curve shows a dispersion-like shape similar to that with CW RF-ONP at low power (figure 4). The width of this dispersion curve is proportional to the strength B_1 of the RF field.

The highest ONP value is found at the first oscillation maximum for the highest available B_1 field. It is at least a factor of two higher than the highest value obtained for CW irradiation. For stronger B_1 fields, correspondingly higher values are expected.

The average intermolecular electronic dipole interaction depends linearly on the concentration of the paramagnetic centres. To check whether in our case the triplet state concentration C significantly affects the efficiency of the polarization transfer we varied C over a wide range by lowering the laser intensity stepwise down to 2% of the maximum value. To avoid strong concentration gradients we chose the excitation wavelength in the low energy wing of the optical absorption line. For a concentration independent quantum yield of the cross polarization process one expects the ONP amplitude to be directly proportional to the number of absorbed photons, i.e. the concentration of excited triplet states. In all our experiments this linear dependence was confirmed, hence a polarization transfer efficiency independent of the light intensity is required.

To summarize the main experimental results:

(i) the oscillatory time dependence is determined by one single frequency (figure 6);

(ii) this frequency is independent of the strength of hyperfine coupling [20];

(iii) near resonance it is given by $\omega_1 = \gamma B_1$, and increases off-resonance, but stays below the electronic Rabi frequency $\omega_R = [\omega_1^2 + (\Delta\omega)^2]^{1/2}$ (figure 7);

(iv) oscillation frequency and ONP efficiency do not depend on the resonance field B_P;

(v) in the limit of long RF pulses the width of the ONP line increases proportional to B_1 (figure 10);

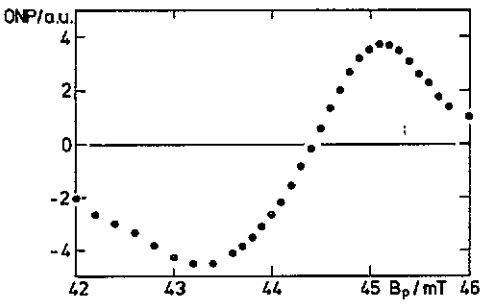

Figure 9. ONP value P_z for long RF pulses ($\tau = 1\ \mu s$, $\omega_1 = 2\pi 25$ MHz, $\nu_{RF} = 120$ MHz) as a function of the polarizing field B_p.

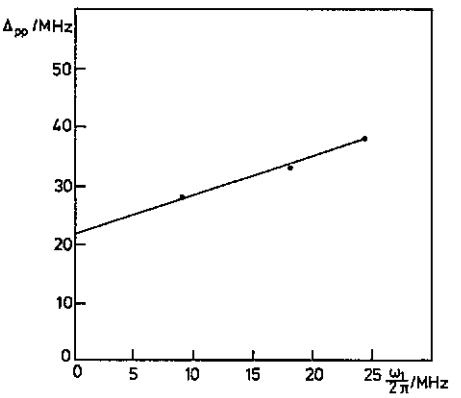

Figure 10. Peak-to-peak line width Δ_{PP} of P_z (B_p) for long pulses as a function of the B_1 fields.

(vi) the sign of the ONP changes with the sign of the offset $\Delta\omega$, for irradiation in the centre of the EPR transition no ONP is generated;

(vii) the ONP level is always proportional to the light intensity.

4.2. Comparison with calculations

The quality of the chosen line shape function $\Phi(\Delta)$ can be tested by calculating the dependence of the peak-to-peak width Δ_{PP} of the RF-ONP line (3.14) as a function of the field strength $B_1 = \omega_1/\gamma$. A linear relationship is obtained in agreement with the experimental data (figure 10). The value extrapolated to $\omega_1 = 0$ corresponds to the width of Φ and yields $\Delta_{PP}(0) = 22.2$ MHz in full agreement with the spectrum in figure 4. A good fit of the asymmetry of Φ is obtained for $\alpha \approx 1$.

For a direct comparison with the experimentally observed ONP oscillations as compiled in figure 6 we calculated the corresponding curves both in the time and frequency domain, as shown in figure 11. The overall agreement is quite satisfying and provides additional evidence for the basic features of the proposed polarization transfer process.

The differences at large off-resonance settings are mainly due to our simplified description of the lineshape. Our assumption of a Gaussian function, slightly modified to take into account asymmetry caused by the non-linear relation between magnetic field and frequency due to zero-field splitting, cannot give sufficiently accurate modelling of the wings, but the wings of the line are of particular importance for irradiation far off-resonance.

In a descriptive way the oscillation spectrum can be made up as a superposition of two parts: one line with ω_1 as centre frequency and a second line with higher frequency components. Roughly speaking, the contributions of all spin packets in the range $\omega_{RF} - \omega_1 < \omega < \omega_{RF} + \omega_1$ add up to the sharp line at ω_1. The second line comprises all other packets; this results in a fast dephasing. As long as we irradiate near the centre of the EPR line we see only the dominant component at ω_1, only for irradiation beyond Δ_{PP} does the second line become dominant. This explains why, for moderate off-resonance irradiation, ω_1 determines the position of the maximum spectral intensity, and further off-resonance the peak value remains at a frequency lower than the Rabi frequency.

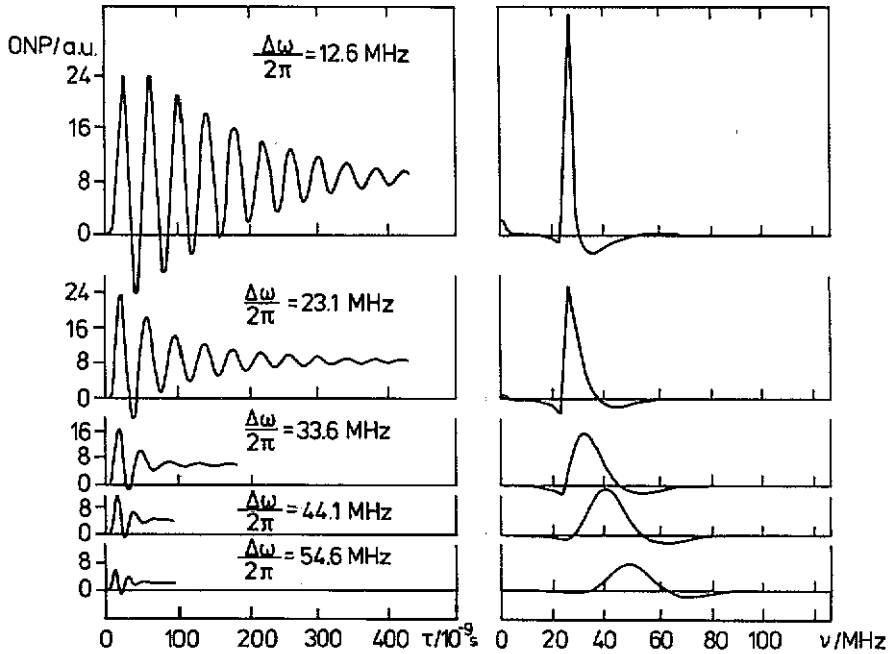

Figure 11. Model calculations for the ONP oscillations adjusted to the experimental parameters in figure 6.

The full curve in figure 7 represents the numerically calculated peak frequencies as a function of the off-resonance settings. The agreement with the experimental values is very good.

4.3. ONP efficiency

It was not the aim of our study to optimize the experimental parameters for maximum polarization. However, in comparison with CW-ONP results it is clear that pulsed RF irradiation will enhance ONP efficiency. For maximum nuclear polarization the crystal system used is not ideal. The quantum yield of the ONP-process is defined as the ratio $\Delta N/N_\lambda$ where ΔN is the net change of population of nuclear spin states and N_λ the number of irradiated photons at wavelength λ. A rough estimate yields the order of 2% for our system. At room temperature the nuclear spin lattice relaxation time under light irradiation is only about 20 s and therefore does not allow a long accumulation of polarization.

However, for such applications where maximum polarization is the main objective, the polarization transfer process described here can be exploited with increased efficiency when the scheme of the RF irradiation is modified according to the following guideline. As the observed ONP is proportional to the non-Zeeman spin energy after the RF pulse, the ideal preparation would correspond to a situation with one half of the EPR line inverted, while leaving the other half unaffected. This may, in practice, not be achievable; however, simple off-centre irradiation of only a single pulse as applied here is certainly rather inefficient in this respect. However, there are comparatively simple pulse sequences which are superior and create a state of the non-Zeeman reservoir

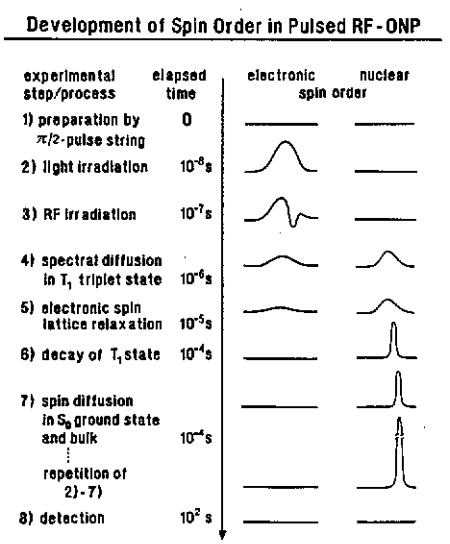

Figure 12. Time development scheme of the ONP process. The spectral shapes on the right side represent the state of electronic and nuclear spin order as a function of the magnetic field.

that needs for its equilibration a higher exchange of energy with the nuclear Zeeman reservoir. In a subsequent publication [56, 57] the application will be described and compared with recently published ONP experiments which use irradiation in the microwave regime (MI-ONP) [58–60]. It shall be mentioned that an analogous transfer scheme can also be used for the coupling of two nuclear spin reservoirs. A demonstration and comparison with the standard method via the Hartmann–Hahn matching condition is given for the case of ^{1}H-^{13}C in solid methanol [61] and hexamethylbenzene [62].

5. Discussion

The emphasis of the reported experiments was on the analysis of the time evolution of electron–nuclear cross-polarization in the submicrosecond time domain and led to a complete, though somewhat simplified scheme, of the whole RF-ONP process. Figure 12 illustrates the time development as divided up into eight separate steps occurring at different time scales, while in reality a significant overlap of individual steps has to be allowed for. In the scheme the state of electronic and nuclear spin order is characterized by the corresponding EPR and NMR line; Boltzmann polarization can be neglected here.

Before the light pulse, all spin polarization was set to zero due to the decay of all excited triplet states and appropriate NMR saturation pulses (step 1). At the end of the laser flash we find the electronic spins highly ordered with a constant polarization level for all spin packets across the inhomogeneous line (step 2). The RF pulses impose a nutation of the triplet spins around $B_{\text{eff}} = (1/\gamma)[\omega_1^2 + (\omega - \omega_{\text{RF}})^2]^{1/2}$, which changes with the frequency position ω of each spin packet. Accordingly, at the end of the pulse, the polarization profile and therefore the spin temperature strongly varies across the line; this resembles the situation of spectral hole-burning, which is well known from CW irradiation schemes (step 3). Spectral diffusion processes tend to re-establish a common spin temperature for all spin packets assumed to occur by energy exchange with the nuclear Zeeman reservoir. Correspondingly, nuclear spin order is generated in the

vicinity of the paramagnetic centre (step 4). Due to electronic spin lattice relaxation the triplet polarization decays; this relaxation can also affect nuclear polarization (step 5). During decay of the triplet to the singlet ground state, nuclear polarization stays unaffected; the disappearance of hyperfine interaction results in a line shift and in an increase of nuclear spin lattice relaxation time (step 6). Spin diffusion in the nuclear spin reservoir leads to a distribution of polarization throughout the host matrix (step 7). The guest molecule is ready for another excitation cycle; in the course of about 10^2 repetitions of steps 2 to 7 nuclear polarization is accumulated. Later the field is changed adiabatically to the higher field of detection, and the magnetization is recorded (step 8).

The basic mechanism of electron nuclear cross-polarization, as revealed by the time-resolved RF-ONP experiments presented here, turns out to be a special case of the thermal mixing concept as developed in solid state DNP [43–46]. As a novel feature, the preparation of high spin order, first in the electronic Zeeman reservoir by light irradiation, then in the electronic non-Zeeman reservoir by RF-radiation, can be done in a pulsed version. As a consequence, the time evolution of the electron–nuclear cross-polarization process can be followed directly. The dominant role of the electronic dipole reservoir as the main contribution to the electronic non-Zeeman reservoir operative in solid-state DNP experiments, with high steady-state concentrations of paramagnetic centres, is found to be insignificant in our case as is expected from the relatively low concentration of optically excited paramagnetic spin states. Efficient thermal mixing between the electronic non-Zeeman and the nuclear Zeeman reservoir is observed nevertheless. No bottleneck shows up owing to inefficient time for the transfer of spin order. In order to compete successfully with the electron spin lattice relaxation a transfer time of the order of 10 μs or faster is required. It can be rationalized as a spectral diffusion process based on double electron, one nuclear, spin flips. As a consequence of the medium range polarization fields used in our experiments this method of spin order transfer may be significantly more efficient as compared to high field experiments.

Acknowledgments

We thank H Zimmermann, Max Planck Institute, Heidelberg, for the synthesis of the isotopically labelled compounds. The financial support by the Deutsche Forschungsgemeinschaft, Sfb 337 (B3), is gratefully acknowledged. DS would like to thank the Institute for Advanced Studies, Hebrew University of Jerusalem, where part of the final work on the manuscript was done during a stay, 1990/91.

References

[1] Abragam A and Goldman M 1978 *Rep. Prog. Phys.* **41** 395
[2] Abragam A and Goldman M 1982 *Nuclear Magnetism: Order and Disorder* (Oxford: Clarendon)
[3] Hausser K H and Stehlik D 1968 *Adv. in Magn. Res.* **3** ed J S Waugh (New York: Academic)
[4] Jeffries C D 1963 *Dynamic Nuclear Orientation* (New York: Wiley Interscience)
[5] Overhauser A W 1953 *Phys. Rev.* **92** 411
[6] Abragam A and Proctor W G 1958 *C. R. Acad. Sci. Paris* **246** 2253
[7] Goldman M 1970 *Spin Temperature and NMR in Solids* (Oxford: Clarendon)
[8] Provotorov B N 1962 *Sov. Phys.-JETP* **14** 1126
[9] Cox S F J, Bouffard V and Goldman M 1975 *J. Phys. C: Solid State Phys.* **8** 3664
[10] Pines A, Gibby M G and Waugh J S 1972 *Chem. Phys. Lett.* **15** 373; 1972 *J. Chem. Phys.* **56** 1776
[11] Maier G, Haeberlen U, Wolf H C and Hausser K H 1967 *Phys. Lett.* **25a** 384

[12] Stehlik D 1977 *Excited States* vol 3, ed E C Lim (New York: Academic)
[13] McArthur D A, Hahn E L and Walstedt R E 1969 *Phys. Rev.* **188** 609
[14] Strombotne R L and Hahn E L 1964 *Phys. Rev.* A **133** 1616
[15] Demco D E, Tegenfeldt J and Waugh J S 1975 *Phys. Rev.* B **11** 4133
[16] Stokes H T and Ailion D C 1977 *Phys. Rev.* B **15** 1271
[17] Müller L, Kumar A, Baumann Th and Ernst R R 1974 *Phys. Rev. Lett.* **32** 1402
[18] Levitt M H, Suter D and Ernst R R 1986 *J. Chem. Phys.* **84** 4243
[19] Müller L and Ernst R R 1979 *Mol. Phys.* **38** 963
[20] Macho V, Stehlik D and Vieth H-M 1991 *Chem. Phys. Lett.* **180** 398
[21] Buntkowsky G and Vieth H-M 1988 *Proc. 10th Ampere Summer School* ed R Blinc, M Vilfan, J Slak (Ljubljana) p 57
[22] Colpa J P and Stehlik D 1972 *Z. Naturforschung* **27a** 1695
[23] Stehlik D, Döhring A, Colpa J P, Callaghan E and Kesmarky S 1975 *Chem. Phys.* **7** 165
[24] Macho V, Colpa J P and Stehlik D 1979 *Chem. Phys.* **44** 113
[25] Macho V 1981 PhD Thesis Free University Berlin
[26] Zhabotinskii M E, Mefed A E and Rodak M I 1972 *Soviet Phys.–JETP* **34** 1020; 1970 *JETP Lett.* **11** 328
[27] Nack M, Stehlik D and Vieth H-M *J. Magn. Res.* submitted
[28] Vieth H-M, Macho V and Stehlik D 1979 *J. Phys. Chem.* **83** 3435
[29] Greene B I, Hochstrasser R M and Weisman R B 1979 *J. Chem. Phys.* **70** 1247
[30] Vieth H-M 1986 *Proc. 7th Spec. Coll. Amp.* (Bucharest: CIP Press) p 61
[31] Rhim W-K, Burum D P and Elleman D D 1976 *Phys. Rev. Lett.* **37** 1764
[32] Gerkin R A, Lundstedt A P and Reppart W J 1984 *Acta Cryst.* C **40** 1894
[33] Belsky V K, Zavodnik V E, Vozzhennikov K M 1984 *Acta Cryst.* C **40** 1211
[34] Grivet J Ph 1971 *Chem. Phys. Lett.* **11** 267
[35] Furrer R, Fujara F, Lange C, Stehlik D, Vieth H-M and Vollmann W 1980 *Chem. Phys. Lett.* **75** 332
[36] Antheunis D A 1974 PhD thesis (Holland: Leiden)
[37] Antheunis D A, Schmidt J and van der Waals J H 1974 *Mol. Phys.* **27** 1521
[38] Vieth H-M 1983 *Chem. Phys. Lett.* **103** 124
[39] Prass B, Fujara F and Stehlik D 1983 *Chem. Phys.* **81** 175
[40] Hartmann S R and Hahn E L 1962 *Phys. Rev.* **128** 2042
[41] Jeneer J, DuBois R and Broekaert P 1965 *Phys. Rev.* A **139** 1959
[42] Deininghaus U and Mehring M 1981 *Phys. Rev.* B **24** 4945; 1979 *Phys. Lett.* **73A** 129
[43] Cox S F J, Bouffard V and Goldman M 1973 *J. Phys. C: Solid State Phys.* **6** L100
[44] Goldman M, Cox S F J and Bouffard V 1974 *J. Phys. C: Solid State Phys.* **7** 2940
[45] Wenckebach W Th, Swanenburg T J B and Poulis N J 1974 *Phys. Rep.* **14** 181
[46] Borghini M, DeBoer W and Marimoto K 1974 *Phys. Lett.* A **48** 244
[47] Melikiya M G 1968 *Sov. Phys. Solid State* **10** 673
[48] Atsarkin V A 1970 *Soviet Phys.–JETP* **31** 1012
[49] Kozhushner M A and Provotorov B N 1964 *Sov. Phys. Solid State* **6** 1152
[50] Buishvili L L 1966 *Sov. Phys.–JETP* **22** 1277
[51] Borghini M 1968 *Phys. Rev. Lett.* **20** 419
[52] Abragam A and Goldman M 1982 *Nuclear Magnetism: Order and Disorder* (Oxford: Clarendon) p 379
[53] Torrey H C 1949 *Phys. Rev.* **76** 1059
[54] Jeffries C D 1960 *Phys. Rev.* **117** 1056
[55] Abragam A 1961 *The Principles of Nuclear Magnetism* (London: Oxford University) Ch 9
[56] Buntkowsky G, Heusinger B, Nack M and Vieth H-M 1988 *XXIVth Congress Ampere* ed J Stankowski, N Pislewski S Idziak (Poznan) D-42
[57] Buntkowsky G, Heusinger B and Vieth H-M 1991 *Appl. Magn. Res.* submitted
[58] Brunner H, Fritsch R H and Hausser K H 1987 *Z. Naturforsch.* **42a** 1456
[59] Henstra A, Dirksen P, Schmidt J and Wenckebach W Th 1988 *J. Magn. Res.* **77** 389
[60] Henstra A, Dirksen P and Wenckebach W Th 1988 *Phys. Lett.* A **134** 134
[61] Vieth H-M, Yannoni C S 1991 *J. Magn. Res.* submitted
[62] Buntkowsky G 1991 PhD Thesis Free University Berlin